Improving the understanding of heat transfer when boiling solid foods

Dat Nguyen

Supervisor: Andreas Håkansson
Examiner: Federico Gomez

LUND UNIVERSITY

LTH
FACULTY OF ENGINEERING

Department of Food Technology, Engineering and Nutrition

ABSTRACT

Determination of the fluid-to-particle heat transfer coefficient h_{fp} is a fundamental problem in food engineering. Solutions to this problem help food technologists and cooks prepare foods with desired characteristics more efficiently in time and energy use. This study aims to determine the h_{fp}-value in simmering and boiling solid foods. Furthermore, it investigates how the culinary terms simmering and boiling corresponds to the pool boiling study in heat transfer literature; and whether they have different impacts on cooking.

Feyissa et al. suggested the method conducted in this study by using potatoes as measuring devices. The study observes the progression of gelatinization over time within potato samples during simmering and boiling to estimate the h_{fp}-values of these cooking practices. It is followed by comparing the experimental travel distances of gelatinization with theoretical values calculated by unsteady-state heat transfer analysis using the Sum of Squared Residuals statistical test. The results show h_{fp}-value of boiling is higher than simmering in the cooking of potato samples. However, this difference does not influence the cooking times significantly due to the limitation in the low thermal conductivity of samples.

These results suggest that the method could estimate the h_{fp}-value of simmering with high certainty. In contrast, another approach is needed to evaluate the h_{fp}-value of boiling with higher precision. Besides, it recommends cooking solid foods by simmering over boiling because of its efficiency in energy use.

ACKNOWLEDGEMENT

I am happy that I made this far with supports from people around me.

I would like to express my deepest appreciation to my supervisor – Andreas Håkansson – for believing in me and being there throughout my academic endeavors at Lund University. I am extremely grateful to his kindness, forthrightness and tremendous support mentally and academically.

Sincere thanks to my girlfriend – Ha Thai, who has always been there through my ups and downs, taking care and providing support to my decisions, whose moral supports and kindheartedness has been invaluable to me.

Special thanks should also go to my best man Duy Tran and Tess who encouraged me to pursuit my study and lead a happy life. I want to also take this opportunity to thank all of my friends – Jasper, Ludvig, Philipp, Ari, Hana, Wiebke, Manon, Ngọc, anh Cuong, anh Tam, anh Vu, chi Linh – who being there with me and made my times in Lund memorable.

My sincerest gratitude goes to my family for always believing in me.

Lastly, this endeavor would not have been possible without the generous support from Swedish Institute, who funded my Master study in Sweden.

TABLE OF CONTENT

I. INTRODUCTION

Boiling and simmering are common food processing practices in a domestic kitchen and industrial production. They originated 30,000 years ago, and historian considers them an important development in the evolution of cooking technology (Speth, 2015). Indeed, they are advancements from the dry cooking method, which uses fire and hot stones to cook foods. In general, these techniques involve the immersion of foods in hot water, whose temperature is close to the boiling temperature of the water.

During boiling and simmering, hot fluids transfer heat to foods and alter their chemistry, sensory and nutritional content. This change continues until the food becomes more edible (McGee, 2004). For example, starchy vegetables have a rigid texture because of their crystalline starch granule content (Sjöö, 2018). Under the presence of heat and water, starch granules disrupt and swell. As a result, the vegetable's texture becomes softer and easier to digest.

A further instance of this is the boiling of meat, in which heat denatures muscle proteins and breaks down connective tissue (McGee, 2004). This modification makes the meat firmer but tender for eating. Most importantly, immersion in water helps maintain the higher moisture content in meat compared to other dry cooking methods such as roasting or grilling.

In food engineering fields, conditions for food processing methods have long been a question of great interest. Knowing how long it takes to cook food and at which temperature could help prepare foods with desired characteristics more efficiently in terms of time and energy use.

Boiling and simmering keep the cooking medium – water – at a temperature close to its boiling point, where the cooking temperature is limited to 100°C and cannot increase further. Thus, the interests simplify to how fast the heat energy is transferred from the hot water medium to the food objects in boiling and simmering. Heat transfer literature quantifies the heat transfer rate in these cases by fluid-to-particle convective heat transfer coefficients h_{fp}.

Previous studies have established that the h_{fp}-value of vessel cooking at 80°C ranges between 100 to 300 W/m^{2}C for food objects of spherical shape (Feyissa *et al.*, 2015). The prediction of h_{fp}-value in vessel cooking was performed by comparing between the gelatinization progression in experiments with theoretical calculations. However, data studies have not determined corresponding h_{fp} values for boiling and simmering conditions. Thus, it is interesting to know whether the Feyissa method applies to these conditions.

In addition, water behaves differently during boiling than when it is not. It is now well established from heat transfer literature that when the temperature difference between the solid heating surface and the boiling temperature of the water increases, water receives higher heat flux from the solid surface (Nukiyama, 1934). Water behaviour alters significantly depending on the amount of heat flux it receives. What is not yet clear is (a) how are these behaviours related to simmering and boiling in culinary practices? And (b)

what are the impacts of these behaviours on the values of h_{fp} in boiling and simmering food?

II. OBJECTIVES

Altogether, the goal of this thesis was to improve the current understanding of heat transfer when boiling food by answering the following research questions:

(1) How do the cooking terms - simmering and boiling - relate to boiling curves in the heat transfer literature?

(2) Is the Feyissa method able to quantify the fluid-to-particle convective heat transfer coefficient h_{fp} of simmering and boiling?

(3) What are the values of fluid-to-particle convective heat transfer coefficient h_{fp} in boiling and simmering that are estimated by the Feyissa method?

(4) What are the implications of these findings in terms of food processing?

It is well established that the values of the convective heat transfer coefficient depend on the geometry of the food. Because of time limitations, this study only investigates a single geometry – a long cylinder with a diameter of 30 mm.

III. LITERATURE REVIEW

5.1. Convective Heat Transfer

Convection is a heat transfer mechanism that occurs in the processing of food.

The mechanism involves heat exchange between solid and fluid by conduction and the transport of heat energy by fluid movement or advection. It happens when there is a temperature difference between the two interfaces and when there is a fluid between the interfaces. Depending on the nature of the fluid motion, either free convection or forced convection is the mode of convective heat transfer between two bodies.

Free convection describes the heat transfer between bodies when fluid motion is solely due to the density gradient created by the temperature gradient during heating or cooling. An example of this phenomenon is the cooling of boiled eggs in cold water. Eggs release heat to nearby water molecules. These molecules begin to move and bump into each other, causing fluid expansion. The heated water becomes less dense and floats to the top. The cold water of higher density gravitates downward to replace hot water, creating a temperature and density gradient in a body of water. Macroscopic movement of fluid continues until the the egg, and surrounding water temperature is in equilibrium.

On the other hand, forced convection describes the heat transfer mechanism when an external factor generates a fluid motion. It can be illustrated by addition of stirring water with a spoon to the previous cooling example. The movement of the fluid around the solid depended not only on gravity but other forces as well. Forced convection transfer more heat than free convection.

Further classification of convective heat transfer considers how fluids flow over the solid surface – or the solid boundary layer. Depending on the viscous properties and velocity of the fluid, the fluid flow in both forced and free convection can be either laminar or turbulent (Singh and Heldman, 2014, p. 285). In the laminar flow, the fluid particles move in order and parallel to each other over the solid boundary. In contrast, fluid flow is highly irregular and moves randomly in turbulent flow (Bergman, Lavine and Incropera, 2017, p. 353).

Regardless of classifications, convection heat transfer study is applicable in various engineering fields, specifically in the food engineering discipline. It helps professionals estimate the time and energy required to process or design conditions to process food. One common approach is to model and solve mathematical equations of physics laws that govern the situation and then compare them with data collected from actual experiments.

5.1.1. Calculation of convective heat transfer rate

Newton's law of cooling describes the mechanism of convective heat transfer mathematically. It states that the total heat loss of a solid body is directly proportional to the temperature differences between the body and its surroundings. The equation is as follows:

$$Q_{convection} = h_{fp}A(Tsolid - Tfluid) = hA\Delta T \qquad \text{Equation 1}$$

$Q_{convection}$ is the heat transfer rate (W) in boiling food, and h_{fp} is the convective heat transfer coefficient ($W/m^{-2}K^{-1}$) between boiling water and suspended food particles. A is the surface area (m^2) where heat transfer occurs; T_{solid} and T_{fluid} are the temperatures at the wall of the food particles and boiling point of water (°C).

From Equation 1, the value of h_{fp} is the most complicated to measure. It depends on the fluid velocity, thermal properties of the hot water, and the physical characteristics of the immersed particles. The quantification of h_{fp} is yet a basic problem in food engineering studies and applications. Knowing the value of h_{fp} allows food engineers to evaluate if operations provide sufficient heat treatment to process foods of interest. There underlies the ability to optimize production efficiency in terms of energy and time consumption.

5.1.2. Estimation of convective heat transfer coefficient by steady-state heat transfer analysis

The first approach to calculate h_{fp} is considering the convective heat transfer is steady-state, which means that the temperature differences between two interfaces are constant with time. For free convection, it is helpful in use the following empirical expression to estimate h_{fp} in free convection (Singh and Heldman, 2014, p. 315):

$$N_{Nu} = \frac{h_{fp}d_c}{k} = a(N_{Ra})^m = a(N_{Gr} \cdot N_{Pr})^m = a(\frac{d_c^3\rho^2 g\beta\Delta T}{\mu^2} \cdot N_{Pr})^m \qquad \text{Equation 2}$$

or

$$h_{fp} = a(\frac{d_c^3\rho^2 g\beta\Delta T}{\mu^2} \cdot N_{Pr})^m \cdot \frac{k}{d_c}$$

These equations include four dimensionless numbers: Nusselt number N_{Nu}, Rayleigh number N_{Ra}, Grashof number N_{Gr}, and Prandtl number N_{Pr}. Accordingly, the Prandtl number is defined as the ratio of momentum diffusivity to thermal diffusivity. Nusselt number is defined as the ratio of convective to conductive heat transfer at a boundary in a fluid. Literature uses Rayleigh number and Grashof numbers to characterize the fluid's flow regime.

On the other hand, d_c is the characteristic dimension of the solid object (m), ρ is the fluid density (kg/m^3). β is the coefficient of volumetric expansion of fluid (K^{-1}). ΔT is the temperature difference between two interfaces, and μ is the absolute viscosity of fluid (Pa·s). Lastly, a and m are coefficients, determined by the geometrical shape of the solid and values of Rayleigh number N_{Ra}.

An example of this is considering convective heat transfer upon a vertical plate. If N_{Ra} is within 10^4 to 10^9, values a and m are 0.59 and 0.25 (Singh and Heldman, 2014, pp. 316–317). By plugging these numbers into Equation 2, h_{fp} of free convection is estimated to be:

$$h_{fp} = 0.59(N_{Ra})^{0.25} \cdot \frac{k}{d_c}$$

Even though this approach is convenient for the estimation, it has the limitation that ΔT is not constant in reality. It decreases from the initial differences to 0°C when the two interfaces are in equilibrium. Thus, Equation 2 estimates h_{fp} at a given point in time, and this needs to be repeated to better understand how it varies throughout the whole heating or cooling process.

When the temperature difference is not constant over time, the literature suggests using unsteady-state heat transfer analysis to quantify the value of h_{fp}. A review of this approach is stated in the following section.

5.1.3. Estimation of convective heat transfer coefficient by unsteady-state heat transfer analysis

Unsteady-state heat transfer analysis considers the heat transfer process where change in temperature within an object is a function of both time and location. This analysis is different from the steady-state one, where temperature differences are constant over time.

The analysis can be done using many different approaches. One is the Heisler chart methodology; another uses simulation tools such as COMSOL. Some of these approaches are limited to situations where h_{fp} is assumed constant over time.

Some approaches to performing unsteady-state heat transfer are limited to cases where the geometry is one of the simplified geometrical shapes. Before the analysis, the geometrical shape of the object is idealized into one of the three optimal shapes, including sphere, finite slab, and finite cylinder. For example, an apple can be considered a spherical object; a potato or water bottle can be viewed as a long cylinder object. A meat patty and a snack bar can be a finite slab shape. However, not all objects are perfectly geometrical. Furthermore, the analysis assumes that the value of h_{fp} is constant, which is not valid. Thus, the approach returns more of an approximation than an absolute solution.

Furthermore, the analysis regards heat conduction in a three-dimensional solid body as a solution to three independent one-dimensional solid body analyses. For example, a long cylinder is a conjunction of an infinite cylinder and an infinite slab; or a finite slab is a conjunction of three infinite slabs. The relation between food temperature and the processing time unfolds by solving equations for each one-dimensional case.

The analysis for one-dimensional heat conduction considers two fundamental equations: (1) the general heat conduction equation and (2) the heat balance equation at the solid-liquid interface. The general heat conduction equation is as follows:

$$\frac{\partial T}{\partial t} = \frac{k}{\rho C_p r^n} \frac{\partial}{\partial r}\left(r^n \frac{\partial T}{\partial r}\right) \qquad \text{Equation 3}$$

Where T is the temperature (°C), t is the time (s), and r is the distance from the central location to the point of assessment (m); k is the thermal conductivity of the solid

($Wm^{-1}K^{-1}$), while ρ and C_p are the density (kg/m^3) and specific heat of the solid ($Jkg^{-1}K^{-1}$). For further calculations, different geometrical shapes have different corresponding values of n. In particular, n = 0 for a slab, n = 1 for a cylinder and n = 2 for a sphere (Singh and Heldman, 2014, p. 356).

The second equation describes the physics that occurs at the solid-liquid interfaces. The rate of heat entering the solid body from the fluid by convection is equal to the amount of inward heat conducting from the surface of the solid. The equation is as follows:

$$At\ r = R: k\frac{\partial T}{\partial r} = h_{fp}(T_{fluid} - T_{surface}) \qquad \text{Equation 4}$$

Where parameter *R* is the distance from the central location to the solid-liquid interface (m), T_{fluid} is the temperature of surrounding fluid (°C), and $T_{surface}$ is the temperature of the solid surface (°C). By setting the boundary conditions where the object's temperature remains constant at t = 0, the analytic solutions of transient conduction in one-dimensional space for three geometrical shapes are obtainable and given below.

For infinite slab:

$$\theta_{infinite\ slab} = \frac{T_{(r,t)} - T_{fluid}}{T_o - T_{fluid}} = \sum_{n=1}^{\infty} \frac{4sin\mu_n}{2\mu_n + sin(2\mu_n)} \cdot e^{(-\mu_n^2 \cdot Fo)} \cdot cos(\mu_n \cdot \frac{x}{L}) \qquad \text{Equation 5}$$

Where *x* is the distance from the centre to the point of assessment, *L* is the distance from the centre to the surface, *Fo* is the Fourier number equal to ht/L^2, and μ_n are positive roots of the transcendental equation (Bergman, Lavine and Incropera, 2017, p. 274):

$$\mu_n \cdot tan(\mu_n) = Bi \qquad \text{Equation 6}$$

For spherical objects:

$$\theta_{sphere} = \frac{T_{(r,t)} - T_{fluid}}{T_o - T_{fluid}} = \sum_{n=1}^{\infty} \frac{4(sin\mu_n - \mu_n cos\mu_n)}{2\mu_n - sin(2\mu_n)} \cdot e^{(-\mu_n^2 \cdot Fo)} \cdot \frac{r_0}{\mu_n r} \cdot sin(\mu_n \cdot \frac{r}{r_0}) \qquad \text{Equation 7}$$

Where *r* is the distance from the centre to the point of assessment in the sphere, *R* is the radius of the sphere, *Fo* is the dimensionless Fourier number equal to ht/R^2, and μ_n are positive roots of the transcendental equation:

$$1 - \mu_n cot(\mu_n) = Bi \qquad \text{Equation 8}$$

For cylinder object:

$$\theta_{infinite\ cylinder} = \frac{T_{(r,t)} - T_{fluid}}{T_o - T_{fluid}} = \sum_{n=1}^{\infty} \frac{2}{\mu_n} \cdot \frac{J_1(\mu_n)}{J_0^2(\mu_n) + J_1^2(\mu_n)} \cdot e^{(-\mu_n^2 \cdot Fo)} \cdot J_0(\mu_n \cdot \frac{r}{r_0})$$ Equation 9

Where the quantity of r, r_0, and Fo is identical to the spherical object and μ_n are positive roots of the transcendental equation:

$$\mu_n \cdot \frac{J_1(\mu_n)}{J_0(\mu_n)} = Bi$$ Equation 10

The quantities of J_0 and J_1 are Bessel functions of the first kind. They can be calculated by the BESSELJ function in Microsoft Excel software or found in textbooks (Bergman, Lavine and Incropera, 2017, pp. 932–934). Values of μ_n are used to approximate transient one-dimensional heat conduction through plane walls, cylinders, and spheres are tabulated in APPENDIX A, Table 1-4.

From these solutions, the relation between time and temperature during the processing of finite objects is mathematically shown as follows (Singh and Heldman, 2014, pp. 366–367):

$$\theta_{finite\ cylinder} = \theta_{infinite\ cylinder} \cdot \theta_{infinite\ slab}$$ Equation 11

And

$$\theta_{finite\ slab} = \theta_{infinite\ slab,width} \cdot \theta_{infinite\ slab,height} \cdot \theta_{infinite\ slab,depth}$$ Equation 12

5.2. Pool Boiling Regimes

Boiling is a changing phase of matter from liquid to vapour at the solid-liquid interface. It occurs when the temperature of the solid surface is higher than the saturation of the liquid. In 1934, Nukiyama studied the correlation between convective heat transfer of boiling with excess temperature between the heating surface and adjacent water (Bergman, Lavine and Incropera, 2017, p. 598).

The study used an electrically heated wire to boil saturated water at atmospheric pressure in a container. The wire is integrated with a resistance thermometer to record its temperature throughout the experiment. The thermometer calibrates electrical resistance in units of temperature. The container is installed with another thermometer to record the water temperature and determine the excess temperature during the heating. From the measured current and voltage supplying to the wire, it was possible to register the heat flux values and obtain the correlation for water at atmospheric pressure, as illustrated in the boiling curve below (Çengel, 2003, p. 518).

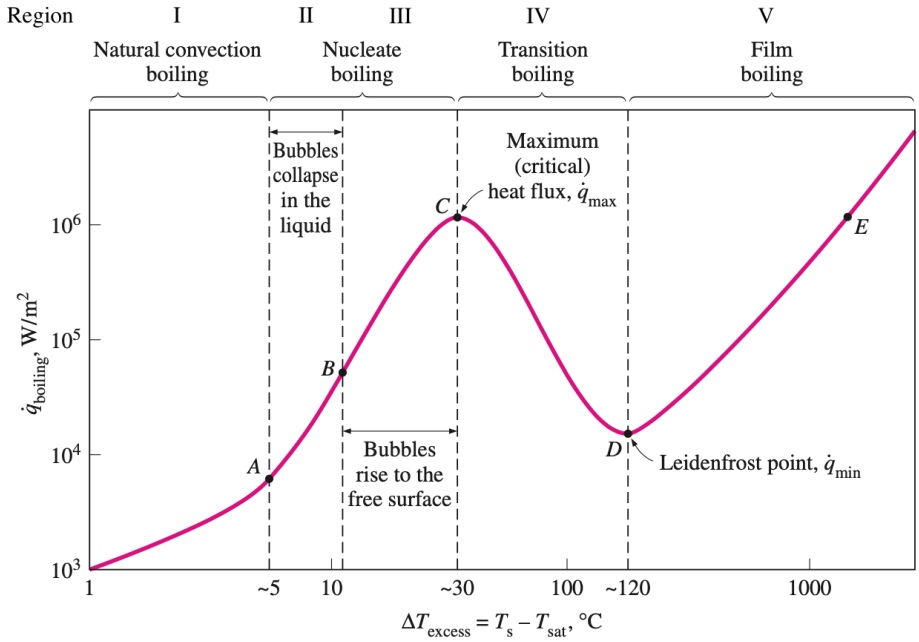

Figure 1: Water's boiling curve at atmospheric pressure (Çengel, 2003, p. 518).

Figure 1 displays the schematic boiling curve of water at atmospheric pressure (Çengel, 2003, p. 518). The scheme divides into five different regions, where the physical mechanism and heat flux change as we increase temperature differences. Y-axis presents the heat flux, and X-axis shows the temperature difference between solid-liquid interfaces.

In Region I in Figure 1, free convection is responsible for fluid motion in the container. The heating surface heats the adjacent liquid to a temperature higher than its boiling point without boiling. The phenomenon is referred to as superheating or boiling retardation. Hot fluid molecules with a lower density rise to the liquid-vapour interface, while cold fluid molecules sink toward the bottom because of gravity (Nukiyama, 1934). The heat transfer in this region can be calculated using the free-convection equations presented in section 5.1.1.

Region II in Figure 1 is the onset of nucleate boiling of the boiling curve. Vapour bubbles begin to form on the heating surface because of evaporation. Depending on the temperature difference on the x-axis, the phenomenon of bubble nucleation occurs differently.

The bubbles may slowly nucleate from the solid surface before collapsing in the liquid. In region II, bubbles rise and move further away from the surface. When bubbles are surrounded by lower-temperature fluid, they dissipate as heat conducts out due to temperature differences. In this region, the heating surface temperature is higher than the boiling temperature of the fluid by 5 to 10°C (Nukiyama, 1934).

As the temperature increases, rapid vapourization begins in region III in Figure 1. Vapour bubbles form faster, merge, and create streaks of vapour to leave the hot surface in the form of jets or slugs. Bubbles rise to the liquid-air interface to release the energy. Free convection no longer governs the fluid motion in regions II and III. The agitation caused

by bubble formation and the vapour transport of energy into the liquid body leads to a higher heat-transfer rate observed in boiling (Nukiyama, 1934).

As the heating surface temperature increases further, the boiling curve enters the IV zone in Figure 1. Bubble formation happens so rapidly that they merge into a vapour layer covering the surface. The heat from the solid surface transfers through the film layer before reaching the liquid and influences the boiling process. The heat transfer rate decreases as the temperature differences increase because the vapour film has lower thermal conductivity than the liquid. Heat transfer reduction continues until the stable vapour film establishes as in Region V. From there, heat transfers from the heating surface to the liquid, governed by solid to vapour conduction and radiation. Radiation through the vapour layer becomes significant as the temperature difference increases. Consequently, the heat transfer rate increases when the temperature of the heating solid increases (Nukiyama, 1934).

In the boiling curve, the heat flux varies between 10^3 to 10^6 W/m^2 depending on the region of interest. Water's critical heat flux – or the highest heat flux – is expected to be 10^6 W/m^2 (Nukiyama, 1934). It occurs right before the curve enters region IV in Figure 1 and is desirable in many engineering applications.

5.3. Heat Transfers in Boiling Foods

Boiling, simmering, and blanching are common practices in cooking food with water at a temperature close to its boiling point.

Presuming cooking food in the pot filled with water by a heating plate. Before cooking, all the listed elements are in temperature equilibrium. Thus, no heat exchange occurs due to a lack of temperature differences. However, when the plate starts to heat the pot, the following heat transfer mechanisms simultaneously cook the food.

Electricity heats the surface of the heating plate according to Joule-Lenz Law. The temperature increment creates the temperature differences between the surface and the bottom of the pot in contact with it. Heat flows from the plate to and within the pot by the unsteady-state conduction mechanism. The temperature changes in the pot's bottom is a function of both location and time.

Heat diffuses through the pot and reaches the pot-fluid interfaces. On the outer surface of the pot, heat conducts to the air adjacent to the pot's sides. Due to density differences and pot cooling from the side, the air circulates onward. On the other hand, at the inner surface of the pot, heat flows to the fluid closest to the bottom by conduction and onwards to the rest of the fluid by convection. Depending on the temperature excess between the bottom of the pot and the adjacent water, different fluid flows and convective heat flux intensity occur according to the pool boiling regimes described in the previous section.

In culinary practice, the identification of a boil is the formation of large bubbles by evaporation at the bottom of the utensils that rise to the surface. Keeping it boiling helps the bubbles at the bottom grow faster. Bubbles coalesce with each other and promote the

vigorous movement of water at its boiling point. On the other hand, a simmer is a water bubbling gently in the cooking pot (Culinary Institute of America, 2011).

5.4. Measuring fluid-to-particle heat transfer coefficient in boiling food

Different methods have been proposed to estimate fluid-to-particle heat transfer coefficient h_{fp} in food processes. A common approach fits the time-temperature profile of processing food particles with the time-temperature curve generated by mathematical solutions of transient heat conduction differential equations in solid bodies. The estimation of h_{fp} is by inversely calculations using Biot number and Fourier number in the transient analysis as described in section 5.1.3 (Lamberg and Hallström, 1986; Denys, Pieters and Dewettinck, 2003).

Two examples of using this approach are the determinations of h_{fp} in blanching of potatoes and pasteurizing of eggs by Lambert in 1986 and Denys in 2003. Both studies used thermocouples injected into different positions in the study objects to record their temperature profiles during processing. Objects' geometries were adapted to simulation models for mathematical calculations. The model presumed fluid-to-particle heat transfer coefficients and predicted the temperature profiles at positions corresponding to the positions of thermal probes in the experiment. By correlating experimental data with theoretical calculations, the estimation of the heat transfer coefficients was possible in these studies.

Another study suggested using a progression of the gelatinization from the surface of the potato to its centre as the indicator for temperature changes in potatoes during cooking with water (Feyissa *et al.*, 2015). This technique is based on the texture kinetics of potato starch gelatinization during heating.

Starch gelatinization occurs when water penetrates and disrupts starch granules in heat. In gelatinization, water diffuses to the amorphous regions of granules composed of single branched amylose, leading to the swelling phenomenon. The heat disrupts the crystalline regions consisting of the highly branched amylopectin, allowing water engaging to hydrogen bonding in the starch molecules (Hans-Dieter, Werner and Peter, 2009). When the potato starch is heated to a degree of gelatinization of about 67.5°C, this bonding causes the starch to become visually more transparent.

The gelatinization reaction happens slowly when $T < T_{gelatinization}$. However, it accelerates when T reaches $T_{gelatinization}$. The visual distinctions between gelatinized and non-gelatinized starches are clear and easy to differentiate upon investigation as shown in the Figure 2 below (Feyissa *et al.*, 2015). The outer ring in the image (a) and (b) are gelatinized region of potato after cooking. Without iodine treatment, this region is more transparent than non-gelatinized region in the image (a). At the same time, it reacts with iodine and is presented as the brown-orange ring on the image (b).

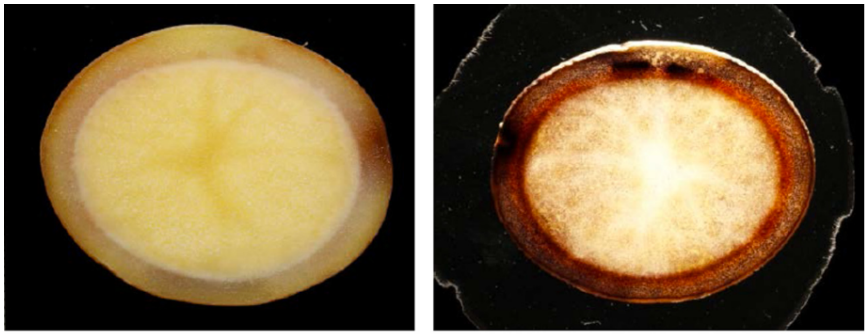

Figure 2: Image of sliced sample without iodine treatment and (b) image of sliced sample stained with iodine treatment (Average diameter = 38mm)(Feyissa et al. 2015).

On the other hand, other cooking indicators have also been suggested by different researches to observe temperature changes within vegetables objects during cooking. These indicators might be identified either before or after than starch gelatinization happening in vegetables. For example, the Gomez-Galindo method consider the inactivation of H^+-ATPase in damage cell of carrot – which occurs before starch gelatinization – as the cooking marker (Gómez *et al.*, 2004). However, due to time constraints, this project only conducted Feyissa method as the cooking marker for further calculations.

IV. MATERIALS AND METHODS

This study observes the progression of gelatinization in potato tubes caused by cooking in boiling and simmering water to estimate the corresponding fluid-to-particle heat transfer coefficient h_{fp} using unsteady-state heat transfer analysis.

The calculations are validated by repeating the observation using 85°C and 90°C water to estimate h_{fp} by unsteady-state heat transfer analysis and Grashof correlation from Equation 2. If calculated values from the two approaches are similar, it is proven that the unsteady-state heat transfer analysis is reliable for predicting h_{fp}.

To obtain experimental data, potato samples were cut into identical cylinder shapes before cooking them in hot water for different time intervals. The samples were cooled by immersing in ice bath immediately after heating. Subsequently, cutting the cooked sample in half allows the identification of the border between the gelatinized and non-gelatinized parts of the sample as the result of cooking. Measuring and then correlating the distance travelled by the gelatinization boundary between different heating times will map the actual gelatinization progress of the potato over time during boiling and simmering (details are discussed in the next section).

Unsteady heat transfer analysis was applied to predict the h_{fp} corresponding to the experimentally observed gelatinization progress for the theoretical calculations. It first assumes h_{fp} and other parameter values for the water and potato samples to calculate the value of the Fourier number using an infinite series. These parameters include water temperature during cooking, initial temperature, and gelatinization temperature of potato samples.

In this analysis, temperature changes in an object is the function of both time and location. Therefore, each Fourier number is associated with a specific heating time required for a specific gelatinization progression distance. Hence, changing the position of the gelatinization in the equations leads to new values of heating time. The theoretical gelatinization progress for different h_{fp} and heating conditions is plotted.

By comparing experimental data and theoretical values, I could determine the h_{fp} of cooking with hot water. On the other hand, the method of quantifying h_{fp} proposed by previous research is validated for boiling water conditions.

The study uses Belana potatoes from Lidl Sverige Supermarket for the experiments because of their size and availability from January to April. Samples are stored at a room temperature of 25°C for 14 days and 28 days before the experiments. Thermophysical properties were quantified since these values are used to plug in the theoretical predictions.

4.1. Thermophysical properties of the potato

The study measures the thermophysical properties of 20 potatoes in total. Ten were 14-day-old, and ten were 28-day-old as presented in their original packaging. Besides recording

the sample properties, the study also aims to clarify if potatoes of different harvesting dates share similar properties and thus, can be used interchangeably.

Quantification of the density of the selected trait is performed by the volume displacement method using the formula $\varrho = m/V$, where ϱ means density (kg/m^3), m means mass (kg), and V means volume (m^3). Ten potato samples were cut in identical shapes before measuring their masses using a balance scale. Then, each sample was submerged in 500mL measurement tubes to find its volume. The amount of water displaced by sample submersion in water equals the samples' volume.

The dual-probe device Thermal Properties Analyzer KD2 quantified the thermal properties of the potatoes. These properties include thermal conductivity, thermal resistivity, thermal diffusivity, and volumetric specific heat. The analyzer records thermal properties by the transient line heat source method (Decagon Devices Inc, 2016, p. 2). It works by injecting two parallel probes into a subject of interest. The first probe generates heat from electricity, causing a temperature increase in the measuring subject. The second probe records the temperature increment over the heating period. The time response of the recorded temperature change is a function of the thermal conductivity of the subject.

4.2. *Water heating set-ups*

Water is heated by an electric hot plate or a temperature-regulated water heating tank. Using a hot plate is to obtain experimental data of simmering and boiling potato samples to estimate h_{fp} using unsteady-state heat transfer analysis.

To estimate the heat flux supplied to the water during cooking, the study uses a power meter to record the amount of power provided to the hot plate. Fill the pot with distilled water and select the power setting on the hot plate. The power meter begins to record when the water is constantly simmering or boiling for at least 2 minutes. Measurements continued for 30 minutes. Assuming that there are no losses between power input and the pot bottom plate. The heat flux coming into the pot equals the record total power supply divided by the total measurement time.

On the other hand, using a water tank is to obtain data of cooking samples in free convection – hot water at 85°C and 90°C. This idea is to validate the method of estimating h_{fp} in a hot plate by comparing results from unsteady-state heat transfer analysis and Grashof-correlations.

The water temperature in these experiments was measured by positioning a K-type thermocouple at a point located 5 centimetres above the bottom of the pot or the water tank.

4.3. Observation of gelatinization progression in potato

The experiment starts by cutting a potato sample into the same cylindrical shape with a diameter d = 30 mm and length L = 50 mm.

It is followed by immersing samples in four different water conditions: boiling, simmering, water at 85°C, and water at 90°C. For each situation, samples are heated for 1-minute, 2-minute up to 6-minute intervals separately. Four samples were prepared for each interval heating.

Afterwards, Samples were placed in an ice bath to stop the heating before cutting them in half to measure the distance of gelatinization progression using a digital caliper. The progression distances were reported as the average of four samples per experiment with standard deviations.

4.4. Determination of hfp of boiling and simmering by unsteady-state heat transfer analysis:

The study uses unsteady-state heat transfer analysis to estimate the convective heat transfer coefficient h_{fp} of simmering and boiling potato samples. Assumed values of h_{fp} are required to perform the analysis that plot the theoretical gelatinization progression resembling the experimental data.

The analysis starts by assuming the geometrical shape of potato samples to be an infinite cylinder. The general temperature profile of the sample is calculated by Equation 9 and Equation 10 as follows:

$$\theta_{potato} = \frac{T_{(r,t)} - T_{fluid}}{T_{potato,initial} - T_{fluid}} = \sum_{n=1}^{\infty} \frac{2}{\mu_n} \cdot \frac{J_1(\mu_n)}{J_0^2(\mu_n) + J_1^2(\mu_n)} \cdot e^{(-\mu_n^2 \cdot Fo)} \cdot J_0(\mu_n \cdot \frac{r}{r_0}) \quad \text{Equation 9}$$

$$\mu_n \cdot \frac{J_1(\mu_n)}{J_0(\mu_n)} = Bi \quad \text{Equation 10}$$

Where r_o = 15mm is the radius of the potato sample; r is the distance between the gelatinization border and the centre of the potato. T_{fluid} is the water temperature; $T_{(r,t)}$ is the temperature of the sample at the position of the gelatinization border. Values of $T_{(r,t)}$ are assumed to be within the range of gelatinization temperature of potato, between 65°C and 67°C. Lastly, h_{fp} is the fluid-to-particle heat transfer coefficient, which assumingly ranges between 500 and 10000 $Wm^{-2}K^{-1}$.

Table 1 below summarize assumed values for T_{fluid}, $T_{(r,t)}$, h_{fp}, and r used for the analysis.

Table 1: Assumed values for unsteady-state heat transfer analysis

Parameter	h_{fp} $(Wm^{-2}K^{-1})$	T_{fluid} (°C)	$T_{(r,t)}$(°C)	*r (mm)*
Assumed values	500, 1000, 2000, 3000, 5000, 10000	To be measured.	65°C, 66°C, 67°C	From 1mm to 15mm

Using different values in Table 1, Equation 9 transforms into different equations corresponding to different heating conditions. Table 4, Table 5, and Table 6 present a complete set of equations in the result section.

In this analysis, each equation is a function of both time and location. Thus, the change in progression distance of gelatinization *r* in Equation 9 correlates with the change in heating time presented by Fourier Number *Fo*. These equations help calculate a specific heating time required for a particular gelatinization progression distance. Altogether, the theoretical gelatinization progression using different set of assuming values for h_{fp}, T_{fluid}, and $T_{(r,t)}$ will be plotted; and used to compare with experimental data.

Calculations of each infinite series equation start with the first term at n = 1, then increasing n to infinite. The increment of term stops only if the solution to the Fourier number is higher than 0.2. The error of the solution is said to be less than 2%, so that we can neglect all remaining terms (Çengel, 2003, p. 218).

From collected values of Fourier number, the heating time required for a specific distance of gelatinization progression is calculated as the following equation:

$$Fo = \frac{\alpha t}{r_o^2} \leftrightarrow t = \frac{Fo \cdot r_o^2}{\alpha}$$

Where *a* is the thermal diffusivity (m^2s) measured in section 4.1. Afterwards, we plot a line graph of the Gelatinization Progression over Heating Time which contain experimental data observed in section 4.3 and theoretical data calculated above.

This study complements graph comparison with Residual Sum of Square statistical analysis to find the model that fits the most with the experiments. To indicate the results, the smaller the value of the Sum of Squared Residuals (SSR), the better the fit of the calculated model.

4.5. Validation of method

4.5.1. Validation of assumption of infinite cylinder geometry

The unsteady-state heat transfer analysis assumes the geometrical shape of potato samples to be an infinite cylinder. This assumption is not applicable in reality. However, the samples' shape resembles the finite cylinder shape. Thus, to validate the comparison stated in the last paragraphs of the previous sections, the temperature profile of an infinite cylinder must represent its long cylinder shape samples prepared in the experiments.

The correlation between the two temperature profiles is expressed in Equation 11.

$$\theta_{long\ cylinder} = \theta_{infinite\ cylinder} \cdot \theta_{infinite\ slab} \qquad \text{Equation 11}$$

The values of $\Theta_{infinite\_slab}$ are estimated using the Heisler chart using calculated values of Fourier number and presuming values of Biot number in section 4.4. In all cases, $\Theta_{infinite\_slab}$ tend to meet the value of 1. Thus, the comparison is reliable.

4.5.2. Validation of unsteady-state heat transfer analysis

This estimation method uses a non-steady-state heat transfer analysis in boiling because no recognised empirical correlations exist. However, there is an empirical correlation for free convection, where the fluid is hot but not agitated by bubble flotation. Hence, in addition to boiling and simmering experiments, the study includes the experiments under the free convection condition to validate the method.

The validation process estimates the h_{fp} of cooking samples at 85°C and 90°C water using both unsteady-state heat transfer analysis and Grashof correlation from Equation 2. It is followed by comparing the results of the two study. If calculated values from the two approaches are similar, it is safe to say that the unsteady-state heat transfer analysis is reliable for predicting h_{fp}.

V. RESULTS

5.1. Primary results

Primary results in this study include thermophysical properties of potatoes measured as described in section 4.1; characteristics of simmering and boiling food observed when performing the experiments described in section 4.3, and results of the h_{fp} experiment.

5.1.1. Thermophysical properties of the potatoes

It is impossible to ensure that potatoes have identical thermophysical properties after the harvest. Therefore, it was interesting to study to what extent these properties vary with storage time.

Table 2 presents collected data on the thermophysical properties of 14-day-old potatoes and 28-day-old potatoes.

Table 2: Thermophysical properties of 14-day-old and 28-day-old potato samples

nr	*Storage Time (days)*	*Thermal conductivity ($Wm^{-1}K^{-1}$)*	*Volumetric specific heat ($Jkg^{-1}K^{-1}$)*	*Thermal diffusivity (m^2s^{-1})*	*Thermal Resistivity (mKW^{-1})*
1	28	0.632	4.02	0.157	158
2	28	0.541	4.10	0.132	184
3	28	0.542	3.77	0.143	184
4	28	0.550	4.22	0.130	181
5	28	0.571	3.97	0.144	175
6	28	0.546	4.39	0.124	183
7	28	0.557	4.39	0.127	179
8	28	0.609	4.49	0.135	164
9	28	0.562	4.31	0.130	177
10	28	0.566	4.90	0.116	176
11	14	0.548	4.10	0.134	182
12	14	0.568	4.35	0.130	175
13	14	0.551	4.22	0.130	181
14	14	0.564	4.32	0.130	177
15	14	0.547	4.20	0.130	182
16	14	0.575	4.08	0.141	174
17	14	0.575	4.18	0.137	173
18	14	0.553	4.17	0.132	180
19	14	0.548	4.69	0.117	182
20	14	0.550	3.99	0.138	181

To test the differences between average values of parameters between 2 sample sets, sample t-tests for an unequal and equal variance were performed. APPENDIX B presents t-values and p-values for each of these tests. Results indicate no statistically significant difference between the means of parameters between two sample sets of different harvest

dates. For that reason, unsteady-state heat transfer analysis could use mean values of parameters from two dates interchangeably for the calculations. Table 3 summarizes the mean values for different parameters for later analysis with their standard deviations.

Table 3: Thermophysical properties of the potatoes

Parameter	*Value*	*Std. Dev (n=20)*
Thermal conductivity ($Wm^{-1}K^{-1}$)	0.562	0.016
Thermal resistivity (mKW^{-1})	177	4.91
Thermal diffusivity ($10^{-6}\ m^2s^{-1}$)	0.132	0.00749
Volumetric specific heat ($Jkg^{-1}K^{-1}$)	4.24	0.257

The volume displacement experiment measured the average density of selected potato traits to be 1.03 ± 0,0085 (kgm^{-3}) (n = 10).

5.1.2. Characteristics of simmering

In simmering experiments, the study measures water temperature at a point located 5cm above the pot's bottom to vary between 97 and 99°C with the mean value of 97±0.5°C. The power supplied to the 20-cm-diameter pot was measured to be 1225±10W, which is equivalent to the supplied heat flux of 39000W/m^2.

Figure 3 shows a picture of a potato sample immersed in a gently simmering water condition. The figure shows that vapour bubbles form at multiple sites at the pot's bottom before floating to the free surface on top. Observing the evolution over time shows a slow bubble release from the nucleation sites, changing the fluid motion within the pot. The potato sample did not stand still but vibrated and then moved slowly around the bottom of the pot when simmering under the influence of buoyancy force created by bubbles flotation.

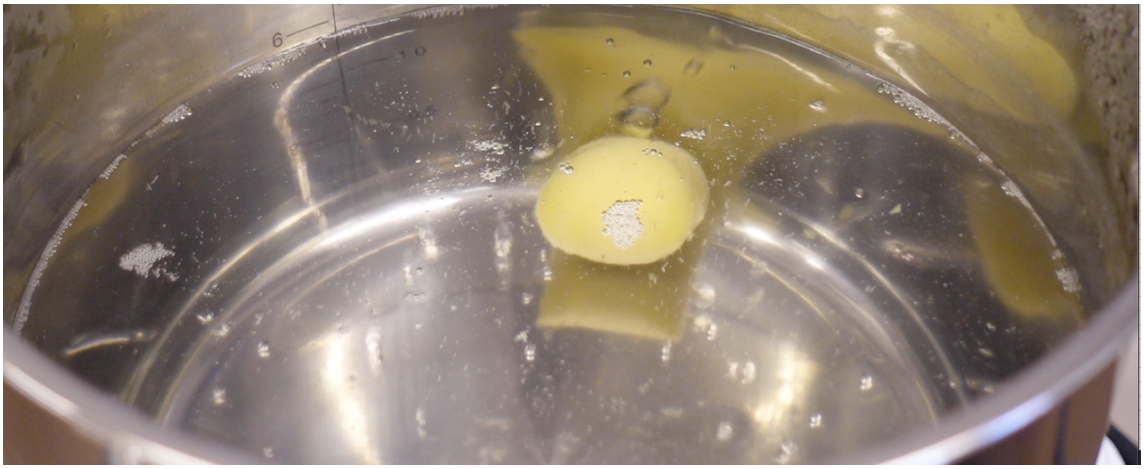

Figure 3: Characteristics of simmering food

5.1.3. Characteristics of boiling

During boiling, a heating plate heats water to its boiling point. The study measures water temperature at a point located 5cm above the pot's bottom to be at its boiling point of 100±0.2°C. The power supplied to the 20-cm-diameter pot was measured to be 1300±24W, which is equivalent to the supplied heat flux of 42000W/m^2.

Figure 4 shows a picture of potato samples immersed in boiling water. The figure shows that water moves vigorously within the pot. Also, it is difficult to identify the bubble nucleation sites from the top view compared to the simmering condition. Before the boiling, observation of the evolution over time shows fast bubble formation and release from the pot's bottom. Bubbles coalesce into each other, forming streaks of large bubbles floating to the free surface. These streaks of bubbles agitate the fluid motions that shake and push potato samples around forcefully.

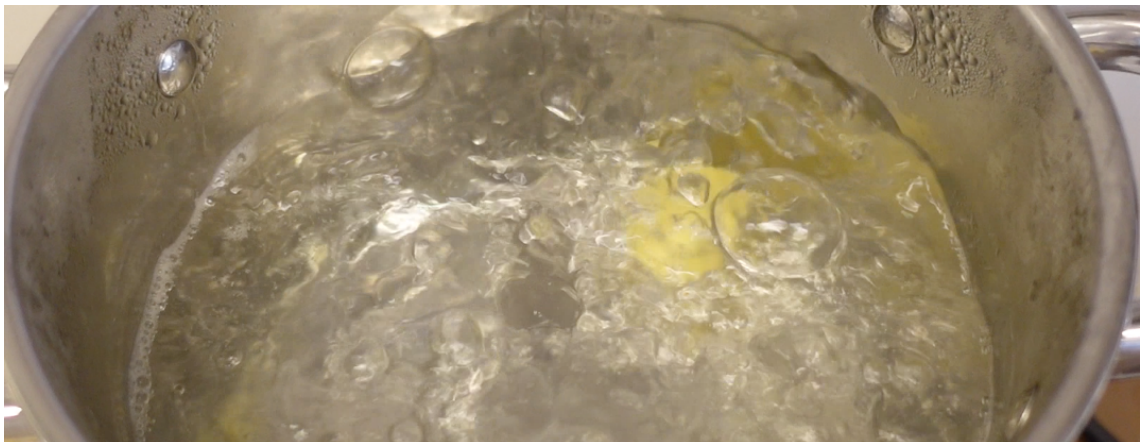

Figure 4: Characteristics of boiling food

5.1.4. Characteristics of sub-boiling

In sub-boiling experiments, a temperature-regulated water bath heats the water to two different conditions, namely 85°C and 90°C. The water temperature at a point located 5cm above the water bath's bottom of two conditions was recorded to be 85±0.5°C and 90±0.4°C, respectively. The study did not take photos and track power usage in these experiments because fluid motion and heat flux during free convection heating with water is not within the objective of this study.

Yet, the fluid constantly moves inside the water tank and shakes the potato samples, but not as significant as in boiling and simmering conditions.

5.1.5. Observation of gelatinization progression in simmering, boiling and sub-boiling

The observation of gelatinization progression in simmering, boiling, and sub-boiling of potato samples was done but cutting the heated potato in half and observed visually. This can be done without any staining, as suggested by Feyissa's method. In general, the gelatinization progression considers changes in the position of the border between the gelatinized and non-gelatinized part of the potato as the effect of changing heating time.

Figure 5 shows the appearance of a sliced potato sample after simmering for 1 minute. As pointed by the red arrow in Figure 5, the gelatinization border separates non-gelatinized and gelatinized regions. The gelatinized regions can be identified visually and look more transparent than the non-gelatinized region.

The gelatinization border progresses further to the sample's centre as the heating time increases. If samples are fully gelatinized, the border is no longer visible. As a result, the progression cannot be tracked, as illustrated in Figure 6.

Figure 5: Image of sliced potato sample after simmering for 1 minute

Figure 6: Image of sliced potato sample after simmering for 5 minutes

Figure 7 compares the effect of heating temperatures on the travel distance of the gelatinization borders in samples prepared as described in section 4.3. Each set of markers presents how the gelatinization border advances over time under specific conditions. Each marker represents the average of 4 observations and the error bar represents the standard deviations of measurements. Data was only available for up to 240 seconds because, after this point, the gelatinization has progressed far enough for the border to become challenging to observe, as illustrated in Figure 6.

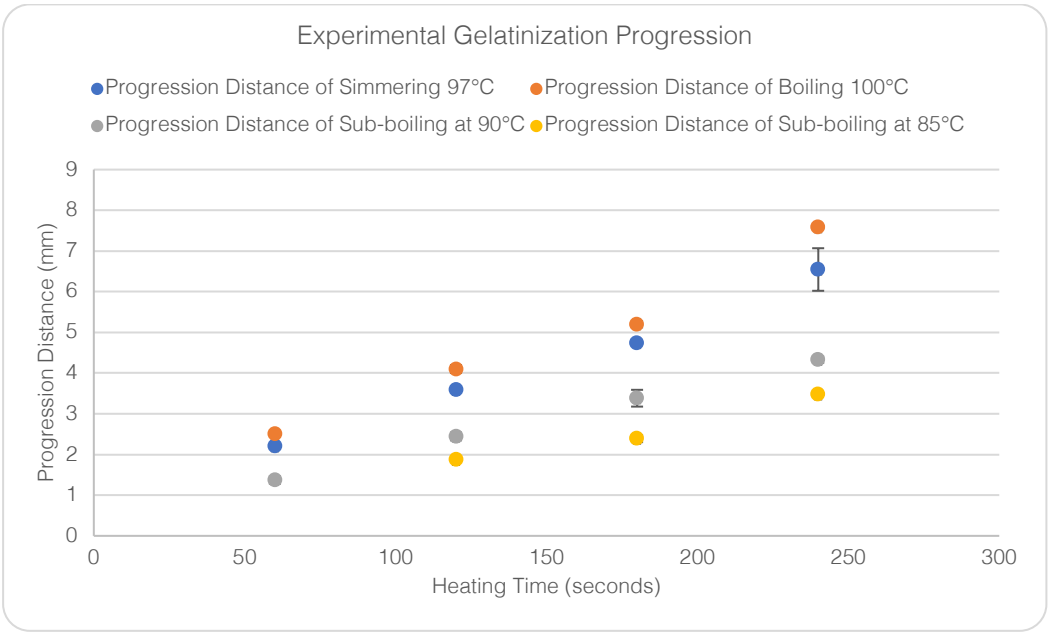

Figure 7: Gelatinization progression of potato in different water conditions

From Figure 7, there is a clear trend of faster gelatinization progression by increasing the fluid temperature.

The figure shows that blanching at 85°C resulted in the slowest progression of gelatinization. The movement is too insignificant that the digital caliper could not register the value within the first minute. On the other hand, the advancement of gelatinization borders in boiling is the fastest, followed by simmering at 97°C. In both cases, borders are difficult to identify from the fourth minute and are entirely gelatinized by the fifth minute, which harnesses further records. This observation is coherent with previous research. They found that when the distance from centre to the gelatinization border is less than 0.6 of the samples' radius, the gelatinization border becomes blurry and difficult to identify (Feyissa *et al.*, 2015).

Interestingly, the data in this Figure 7 shows no significant improvement in heating time reduction when comparing boiling and simmering. Given that the fluid movement in boiling differs from simmering, as shown in 7.1.2, the following section aimed to estimate fluid-to-particle heat transfer coefficients h_{fp} from the observations in Figure 7.

5.2. Secondary Results

Secondary results in this study include (1) the estimations of gelatinization progression theoretically by unsteady-state heat transfer analysis; (2) and comparison between the estimations with experimental data.

5.2.1. Estimation of gelatinization progression using unsteady-state heat transfer analysis:

5.2.1.1. Setting up the temperature profile equation:

The temperature profile equations used water temperature measured in the boiling, simmering and sub-boiling experiments as the values of T_{fluid}. From 5.1.2, boiling has water temperature measured to be 100°C. The temperature of simmering water ranges from 97 to 99°C as presented in section 5.1.3. Lastly, the sub-boiling conditions have the water temperature of 85°C and 90°C, as stated in section 5.1.4.

Table 4, Table 5, and Table 6 below present T_{fluid} with presuming values of h_{fp} and $T_{(r,t)}$ for the unsteady-state heat transfer analysis of boiling, simmering, and sub-boiling, respectively. Altogether, these values transform Equation 9 into 80 different equations describing the heat transfer within potatoes in boiling and simmering experiments. For example, the temperature profile equation corresponding to set number 6 in the table is as follows:

$$\theta_{potato} = \frac{65-100}{20-100} = \sum_{n=1}^{\infty} \frac{2}{\mu_n} \cdot \frac{J_1(\mu_n)}{J_0^2(\mu_n) + J_1^2(\mu_n)} \cdot e^{(-\mu_n^2 \cdot Fo)} \cdot J_0\left(\mu_n \cdot \frac{r}{15}\right)$$

$$\mu_n \cdot \frac{J_1(\mu_n)}{J_0(\mu_n)} = Bi = \frac{hd_c}{k} = \frac{10000 \cdot 7.5}{0.56}$$

Values of thermal conductivity k are taken from the thermophysical properties of potatoes presented in *Table 3*.

Table 4: Complete sets of assuming values for temperature profile of boiling in the unsteady-state heat transfer analysis

Parameter / *Set*	T_{fluid} (°C)	$T_{(r,t)}$ (°C)	h_{fp} (W/m^2C)	*Sum of Squared Residuals*
1	100	65	500	19.0
2			1000	6.4
3			2000	2.5
4			3000	*1.6*
5			5000	*1.4*
6			10000	*1.4*
7		66	500	25.0
8			1000	9.3
9			2000	4.3
10			3000	3.1
11			5000	2.70
12			10000	2.70
13		67	500	32.0
14			1000	13.0
15			2000	6.7
16			3000	5.1
17			5000	4.5
18			10000	4.5

Table 5: Complete sets of assuming values for temperature profile of simmering in the unsteady-state heat transfer analysis

Parameter / *Set*	T_{fluid} (°C)	$T_{(r,t)}$ (°C)	h_{fp} (W/m^2C)	*Sum of Squared Residuals*
19	99	65	500	6.3
20			1000	0.64
21			2000	0.12
22			3000	0.30
23			5000	0.42
24			10000	0.42
25		66	500	9.3
26			1000	1.5
27			2000	0.19
28			3000	0.12
29			5000	0.14
30			10000	0.14
31			500	12.0
32			1000	3.0

Parameter / Set	T_{fluid} (°C)	$T_{(r,t)}$ (°C)	h_{fp} (W/m^2C)	Sum of Squared Residuals
33	98	67	2000	0.70
34			3000	0.34
35			5000	0.25
36			10000	0.25
37		65	500	7.9
38			1000	1.12
39			2000	0.11
40			3000	0.15
41			5000	0.21
42			10000	0.21
43		66	500	11.0
44			1000	2.3
45			2000	0.44
46			3000	0.19
47			5000	0.15
48			10000	0.15
49		67	500	15.0
50			1000	4.1
51			2000	1.2
52			3000	0.70
53			5000	0.54
54			10000	0.54
55	97	65	500	9.8
56			1000	1.7
57			2000	0.25
58			3000	0.12
59			5000	0.13
60			10000	0.13
61		66	500	13.0
62			1000	3.3
63			2000	0.86
64			3000	0.44
65			5000	0.32
66			10000	0.32
67		67	500	18.0
68			1000	5.6
69			2000	2.0
70			3000	1.2
71			5000	1.0
72			10000	1.0

Table 6: Complete sets of assuming values for temperature profile of sub-boiling in the unsteady-state heat transfer analysis

Parameter / *Set*	T_{fluid} (°C)	$T_{(r,t)}$ (°C)	h_{fp} (W/m2C)	*Sum of Squared Residuals*
73	85	65	500	0.95
74			750	0.23
75			1000	4.4
76			2000	6.5
77	90		500	0.12
78			750	0.14
79			1000	0.70
80			2000	1.52

5.2.1.2.Plotting the results of unsteady-state heat transfer analysis:

Temperature profile equations (total of 80) calculate Fourier number by term approximation method. Each equation estimates 8 Fourier numbers corresponding to the first 8mm of gelatinization progression. Heating time is calculated from the mathematical definition of Fourier number. Accordingly, theoretical gelatinization progression by the heating time of 80 equations is presented in scatter plots to compare with experimental data from 5.1.5. The following table presents the comparisons of all equations' solutions with experimented data:

Table 7: Comparison of gelatinization progression between theoretical values and experimental data. Gp_boiling, gp_simmering, gp_85 and gp_90 represent data recorded from boiling, simmering and sub-boiling experiments. h_{fp} = [values] represent theoretical progression for corresponding h_{fp} at specific T(r,t) and Tfluid.

Tfluid	*T (r,t) = 65°C*	*T (r,t) = 66°C*	*T (r,t) = 67°C*
Boiling			
100°C	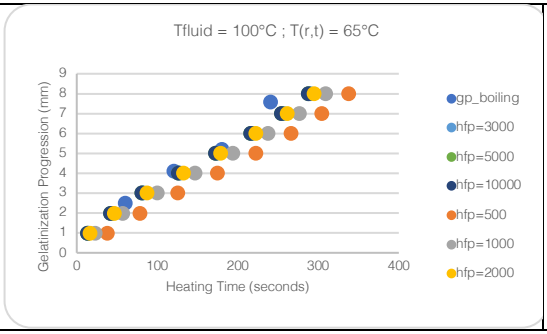	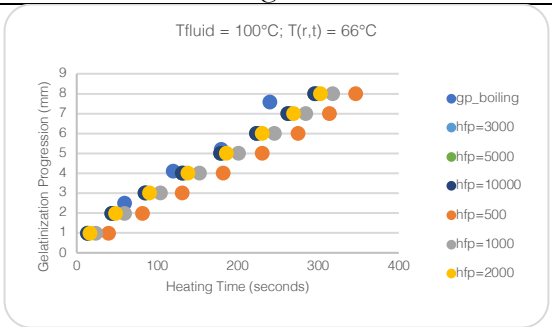	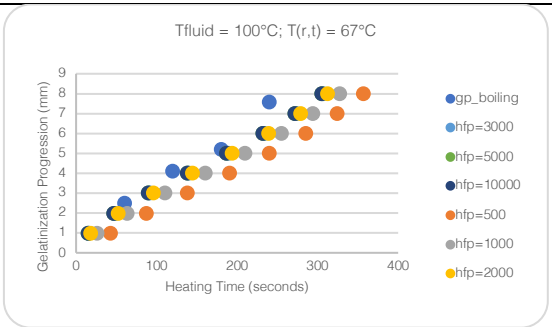
Simmering			
99°C	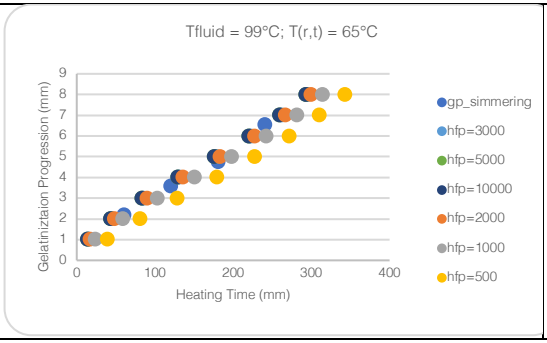	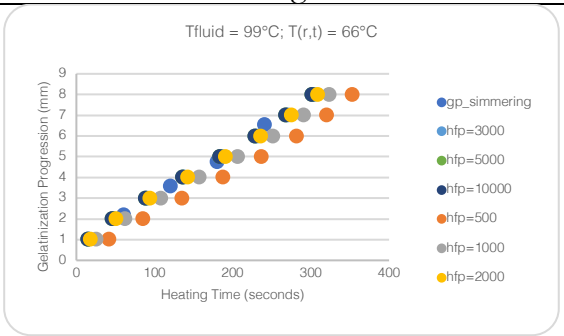	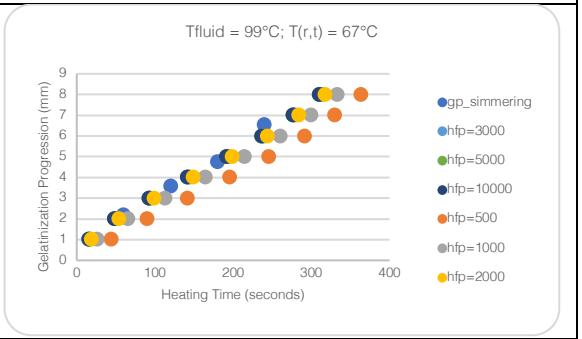

Tfluid	*T (r,t) = 65°C*	*T (r,t) = 66°C*	*T (r,t) = 67°C*
98°C	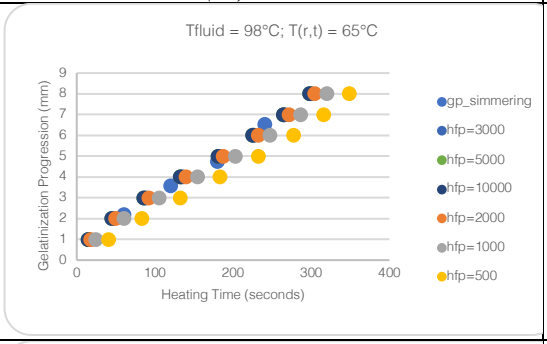	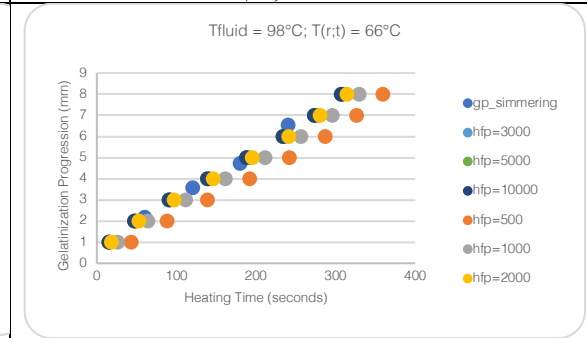	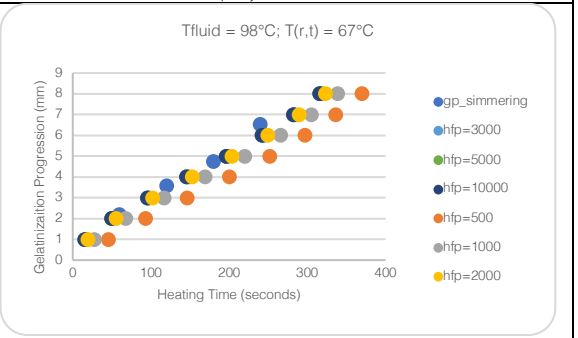
97°C	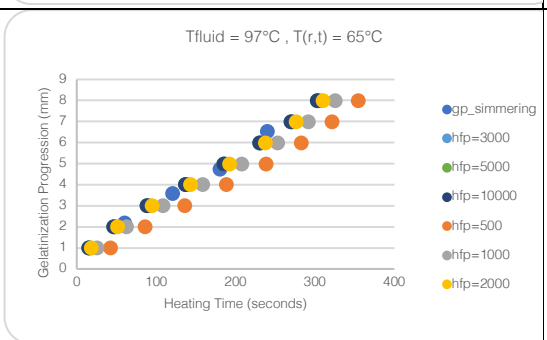	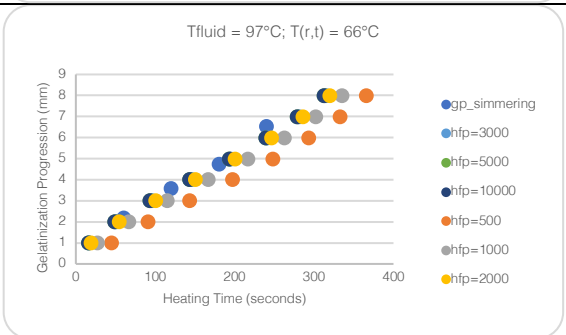	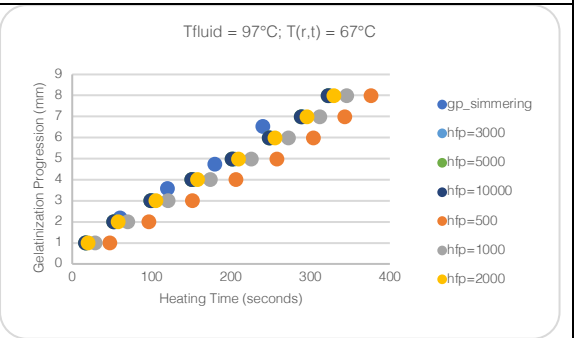
Sub-Boiling			
85°C	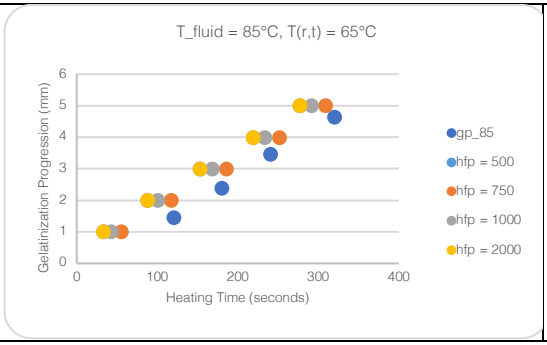		

Tfluid	*T (r,t) = 65°C*	*T (r,t) = 66°C*	*T (r,t) = 67°C*
90°C	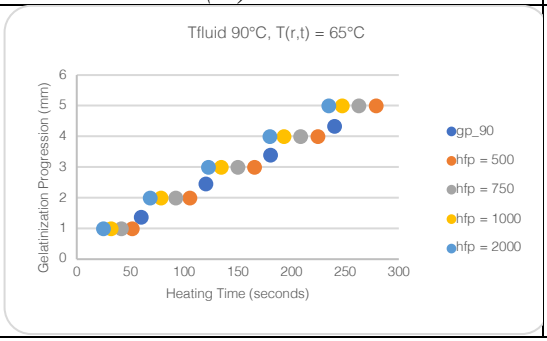		

From Table 7, there are several interesting observations about the calculated heating times regardless of *Tfluid* and *T(r,t)* values. The first observation is the trend of faster gelatinization progression by increasing the h_{fp}-values from 500 W/m²C up to 5000 W/m²C. The further the gelatinization, the higher the difference between the required heating time. At the same *Tfluid* and *T(r,t),* for gelatinization border to move the first millimetre r = 1mm, heating with h_{fp} = 500 W/ m²C often results in 25 to 30 seconds longer than with h_{fp} = 5000 W/m²C. However, when the border moves further to the centre, it takes up to 50 to 54 seconds in heating time difference.

The second observation is the identical progression of h_{fp} = 5000 W/m²C and h_{fp} = 10000 W/m²C in all calculations. This observation is because the left-hand side of the transcendental Equation 10 is identical as the Biot number on the right-hand side is higher than 100 by looking at the table of roots. Meanwhile, the potato samples had small values of thermal conductivity k = 0.56 ± 0.02 W/mK and characteristic dimension d_c of 0.015 m. Thus, any values of h_{fp} that are higher than 3733 W/m²C would result in values of Biot number higher than 100. Therefore, an increase in h_{fp} value does not always correlate with a faster gelatinization process. Altogether, the first two observations suggest the limitation of the method. If the h_{fp} value is higher than 3733 W/m²C, the method cannot estimate the h_{fp} value correctly. It also cannot quantify their difference if h_{fp} is higher than 3733 W/m²C.

When the value of Tfluid is considered, a trend of decreasing gelation progress time is observed as T_{fluid} increases. The trend is similar to the first observation mentioned earlier but of a different magnitude. If the h_{fp} is identical, increasing T_{fluid} by 1°C results in 0.6 to 2-second reductions in the first millimeter of gelatinization progression. As gelatinization progressed further, the improvement was up to 7 seconds.

On the other hand, a different tendency is spotted when considering the impact of changing $T_{(r,t)}$ on calculated heating time. Increasing the $T_{(r,t)}$ alone increases the heating time for the same gelatinization progression by 3 to 10 seconds, depending on the travel distance of the gelatinization border and values of h_{fp}.

5.2.1.3.Comparison between experimental and theoretical gelatinization progression:

Table 7 shows that calculated progressions resemble the experimental progression but differ depending on presuming values of T_{fluid}, $T_{(r,t)}$, and h_{fp}.

Results of the Residual Sum of Square statistical analysis on each of the 80 theoretical progresses are presented in the fifth column in Table 4, Table 5, and Table 6. Analysis of the results for boiling and simmering are shown below. The study also includes the analysis for sub-boiling, which will be included in the following validation section.

The study's first finding is that the higher the h_{fp}, the smaller the values of SSR, regardless of T_{fluid} and $T_{(r,t)}$. These differences can be seen from the scatter plot comparison, where progressions with h_{fp} < 2000 W/m²C deviates significantly from the experimental regression models. This finding suggests that fitted models would have the values of h_{fp} > 3000 W/m²C for both experimental simmering and boiling models.

For boiling models, analysis shows that the conditions with T_{fluid} = 100°C, $T_{(r,t)}$ = 65°C, and h_{fp} > 3000 W/m²C fits well with the regression equations. However, best fits are conditions with h_{fp} of 5000 W/m²C and 10000 W/m²C, where SSRs are equal to 1.4. The scatter plot comparison between the gelatinization progression of these conditions and experimental data is shown in Figure 8 below.

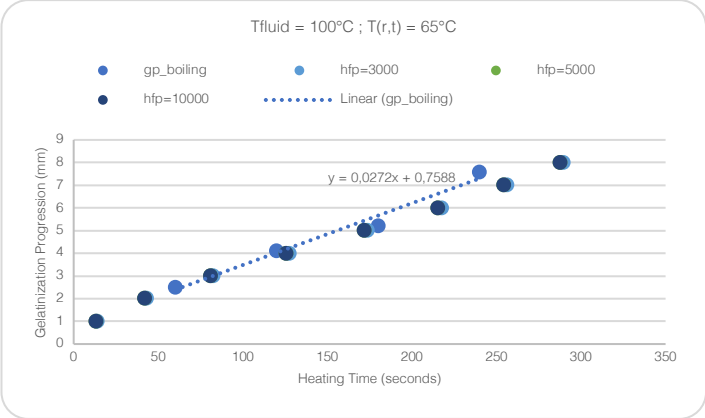

Figure 8: Fitted models for gelatinization progression of boiling

As explained earlier, the method could not quantify h_{fp}-values higher than 3733 W/m²C. Thus, based on this analysis, one could only suggest that the convective heat transfer of boiling in long cylinder particles is higher than 3733 W/m²C.

The SSR calculations suggest several theoretical conditions that fit the reference model regarding the simmering model. Table 8 present a summary of the possible conditions extracted from Table 5.

Table 8: Fitted theoretical gelatinization progression models for simmering by unsteady-state heat transfer analysis

Parameter / *Set n.*	T_{fluid} (°C)	$T_{(r,t)}$ (°C)	h_{fp} (W/m²C)	*Sum of Squared Residuals*
27	99	66	2000	0.198
28			3000	0.120
29			5000	0.140
30			10000	0.140
39	98	65	2000	0.118
40			3000	0.150
41			5000	0.213
42			10000	0.213
58	97	65	3000	0.128
59			5000	0.129
60			10000	0.129

The values of prediction of the fitting model presented in Table 8 are as expected because the water temperature during the simmering experiment ranges between 97 and 99°C rather than staying at the absolute value in boiling. However, the finding also estimated

that h_{fp} to be between 2000 to 3000 W/m²C as the SSRs reduce in this range before increment at h_{fp} equals 5000 and 3000 W/m²C.

Altogether, higher T_{fluid} and h_{fp} contribute to the faster gelatinization progression observed in boiling than in the simmering experiment.

5.2.2. Validation of unsteady-state heat transfer analysis

Unsteady-state analysis was used to estimate h_{fp} when cooking potatoes with 85°C and 90°C water to validate the method in boiling and simmering. This study compares the h_{fp} values of this analysis with values estimated by the Grashof number in Equation 2.

Experimental data of gelatinization progression in potato samples while heating at sub-boiling temperature was presented in section 5.1.5. Unsteady-state heat transfer analysis showed that the convective heat transfer of cooking potato samples at 85°C falls between 400 and 500 W/m²C. Whilst its of 90°C is between 500 to 750 W/m²C. These conclusions are made based on the results of SSRs, as shown in the fifth column of Table 6.

Concurrently, h_{fp}-values of these conditions are estimated by Grashof-correlation at two specific points in time. The first correlation is performed at time t = 0 where $T_{potato\ surface}$ = 20°C, and the second is at the moment when $T_{potato\ surface}$ is differed from T_{fluid} by 5°C. By doing so, we could study how h_{fp} varies in the cooking process. Accordingly, h_{fp}-values of cooking long cylinder potato samples at 85°C were estimated to range between 679 and 1290 W/m²C; and vary between 744 and 1440 W/m²C when cooking at 90°C. In both cases, the high empirical values are results of the correlation at t =0, and low empirical values are results of the correlation at ΔT = 5°C.

The comparison between h_{fp}-values of cooking at free convective conditions estimated by unsteady-state heat transfer analysis and Grashof-correlations are presented in the following Figure 9:

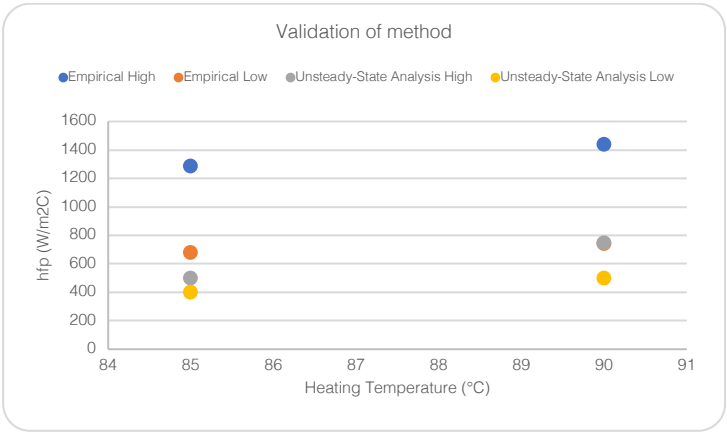

Figure 9: Comparison of h_{fp} in free convection calculated by empirical Grashof-correlation and unsteady-state heat transfer analysis.

Figure 9 shows that h_{fp}-values by Grashof-correlation vary significantly between two points in time. The experimental method results in an h_{fp}-value in the same order of magnitude

as results from empirical Grashof-correlation at the moment where $\Delta T = 5°C$. Thus, the study concludes that the unsteady-state heat transfer analysis is reliable in estimating the h_{fp}-value of long cylinder potato samples.

VI. DISCUSSION

6.1. Relating pot boiling to the boiling curve

As presented in sections 5.1.2 and 5.1.3, the supplied heat flux during simmering was 39000W/m^2. Also, the supplied heat flux during boiling was 42000W/m^2. According to the boiling curve in Figure 1, bubble nucleation boiling happens between 8000 and 70000 W/m^2. This observation suggests that water conditions in both simmering and boiling experiments of this study are in the nucleate boiling region of the curve.

Besides, the slow bubble nucleation at the pot's bottom observed during simmering experiments is similar to the phenomena found within the bubble nucleation zone in the nucleate boiling region. Thus, simmering correlates specifically with this zone in the boiling curve.

In the same way, the study confirms the relationship between the water condition in the boiling experiments with the nucleate boiling region. However, the fluid phenomena suggest it correlates more specifically with the early jet nucleation zone in the boiling curve.

6.2. Methodological discussions

The method was able to predict the progression of gelatinization border as observed in the experiments with samples of long cylinder shapes. Regardless of the heating conditions in the study, the solutions were always a range of h_{fp}-value rather than exact numbers.

For the boiling experiments, h_{fp} was quantified to be higher than 3000 W/m^{2}C. The analysis could not predict precisely the h_{fp}-value because the mathematical prediction of the gelatinization progression becomes identical when h_{fp}-values are higher than 3733 W/m^{2}C. This event happened when the heat transfer inside the long cylinder potato samples was much slower than the heat convection into its surface. In other words, increasing h_{fp} -values from 3733 W/m^{2}C does not show faster gelatinization progression in the prediction. For this reason, the method is not accurate enough to predict h_{fp} in the boiling of the long cylinder potato samples. Indeed, it suggests using other devices with higher thermal conductivity to predict h_{fp} of boiling foods in general.

In the same way, h_{fp} of simmering was quantified to range between 2000 and 3000 W/m^{2}C by using the Feyissa method. Contrary to the limit in the boiling, the study can improve the precision of predicting h_{fp}-value by repeating the analysis with thousands of presuming h_{fp}-values in the range. For example, h_{fp} = {2000.10; 2000.12; …; 2999.99; 3000}. The best-fitted model would have the lowest Sum of Square Residuals value compared to experimental gelatinization progression data. This observation suggests that the Feyissa method is usable in predicting the h_{fp}-value of simmering food particles.

6.3. Implications for food processing practices

From the estimated values of h_{fp} in boiling and simmering, the time required to cook the potato samples of long cylinder shapes can be calculated using either a Heisler chart or term approximation.

By presuming the cooked potato samples have a centre temperature is 97°C, the cooking time by boiling and simmering is calculated and presented by blue markers in Figure 10 below.

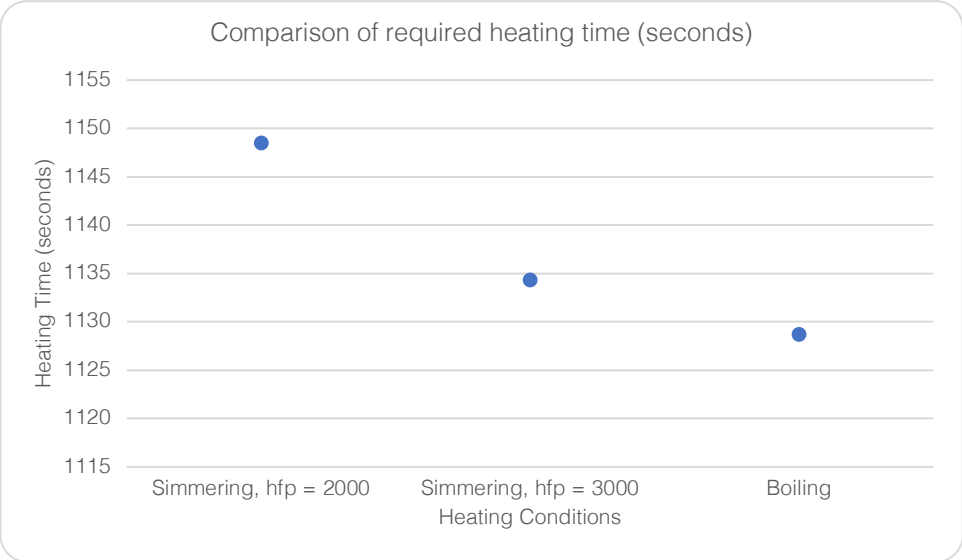

Figure 10: Comparison of required heating time between heating conditions

It can be seen from Figure 10 that boiling cooks the potato samples faster than simmering by 10 to 20 seconds, depending on the h_{fp}-values of simmering. According to sections 5.1.2 and 5.1.3, the amount of power supplied for boiling was 1300±24W, and for simmering was 1225±10W. Because of this, boiling costs 0.016 to 0.021 kWh more than simmering to cook the potato samples. Altogether, one could argue that the energy cost for boiling is substantially higher than simmering, but the cooking time does not noticeably reduce. In other words, cooking food with simmering is more sustainable than boiling in terms of energy efficiency.

Although these results are restricted to the potato samples prepared in section 4.3, the study suggests that they are also applicable to different foods with long cylinder geometrical shapes – for example, carrot, cassava, patty meat, or those whose have low thermal conductivity properties similar to potatoes.

VII. CONCLUSIONS

Conclusions in this study include the answer to each of the four research questions stated in the INTRODUCTION.

(1) How do the culinary practices – boiling and simmering – correlate with the boiling curve in heat transfer literature?

Both simmering and boiling correspond to the nucleate boiling region in the boiling curve. Moreover, simmering correlates with the late bubble nucleation zone and boiling correlates with the early jet nucleation zone in the region.

The bubble nucleation zone is characterized by the slow yet noticeable formation of tiny vapour bubbles at the solid-fluid interface. On the other hand, jet nucleation is characterized by a constant stream of large vapour bubbles that creates vigorous fluid movement.

(2) Is the Feyissa method able to distinguish the fluid-to-particle convective heat transfer coefficient h_{fp} in simmering and boiling?

The Feyissa method can quantify the difference in h_{fp}-values between simmering and boiling for the samples having long cylinder geometrical shapes. Again, when going from simmering to boiling, the h_{fp}-value increases by at least 23%.

(3) What are the values of h_{fp} in boiling and simmering that is estimated by the Feyissa method?

It suggests that the h_{fp}-value of simmering ranges between 2000-3000 W/m^{2}C, and the h_{fp}-value of boiling is equal to or higher than 3733 W/m^{2}C for long cylinder samples.

(4) What implications does this study have in terms of food processing?

To some extent, boiling gives a higher fluid-to-particle convective heat transfer coefficient h_{fp} than simmering. This finding contributes to the reduced cooking time when boiling. However, the reduction is insubstantial regardless of the h_{fp}-values. It is because the internal resistance to heat transfer is higher than the outer resistance in food cooking. Thus, the convective heat transfer coefficient increments do not affect cooking time significantly. Meanwhile, the energy cost increases substantially when switching from simmering to boiling. Indeed, it is more sustainable to cook food of long cylinder geometrical shape by simmering than by boiling in terms of energy uses.

VIII. FUTURE WORKS

First, the method used in this study assumed the geometrical shape of objects of the long cylinder shape. Future studies could investigate the relationship between the geometrical shape of food samples and h_{fp}-values in boiling and simmering conditions. Consequently, results from these investigations extend the applicability of these studies in food processing practices.

Second, this study assumed only six h_{fp}-values for the unsteady-state heat transfer analysis of simmering. A few assumptions were to obtain the general ideas of how theoretical values fitted with experimental data. Considering the analysis predicted h_{fp}-values ranging between 2000-3000 W/m^{2}C, extra h_{fp}-values within this range might need to be considered for more precise and accurate predictions in future studies. Future studies can execute this idea by changing values manually in the calculations on Microsoft Excel or by programming scripts in the mathematical solver of computer programs such as MATLAB or Python.

Third, the Feyissa method used in this study considers starch gelatinization as the marker for heat transfer within potato samples. Future works involves different markers for cooking occurred at lower temperature would yield more accurate data for calculations. For example, potential cooking marker is the inactivation of H^+-ATPase in carrot's damage cell was suggested by the Gomez Galindo method.

Lastly, I believe that apart from looking for results from experimental studies, future research should look for numerical modelling by simulation applications to have a better understanding of the heat transfer mechanism during boiling. I prospect the simulation model must describe multiple physics analyses in the process of cooking. For example, (1) the liquid and vapour flow around the object of interest, (2) the heat transfer between solid and different fluid.

IX. REFERENCES

Bergman, T.L., Lavine, A. and Incropera, F.P. (2017) *Fundamentals of heat and mass transfer*. Available at: https://ebookcentral.proquest.com/lib/qut/detail.action?docID=5106220 (Accessed: 29 April 2022).

Çengel, Y.A. (2003) *Heat transfer: a practical approach*. 2nd ed. Boston: McGraw-Hill.

Culinary Institute of America (ed.) (2011) *The professional chef*. 9th ed. Hoboken, N.J: John Wiley & Sons.

Decagon Devices Inc (2016) *KD2 Pro Thermal Properties Analyzer Operator's Manual*. WA Pullman, USA.

Denys, S., Pieters, J.G. and Dewettinck, K. (2003) 'Combined CFD and Experimental Approach for Determination of the Surface Heat Transfer Coefficient During Thermal Processing of Eggs', *Journal of Food Science*, 68(3), pp. 943–951. doi:10.1111/j.1365-2621.2003.tb08269.x.

Feyissa, A.H. *et al.* (2015) 'Studying fluid-to-particle heat transfer coefficients in vessel cooking processes using potatoes as measuring devices', *Journal of Food Engineering*, 163, pp. 71–78. doi:10.1016/j.jfoodeng.2015.04.022.

Gómez, F. *et al.* (2004) 'Isothermal calorimetry approach to evaluate tissue damage in carrot slices upon thermal processing', *Journal of Food Engineering*, 65(2), pp. 165–173. doi:10.1016/j.jfoodeng.2004.01.010.

Hans-Dieter, B., Werner, G. and Peter, S. (2009) *Food Chemistry*. 4th edn. Berlin, Heidelberg: Springer Berlin Heidelberg. doi:10.1007/978-3-540-69934-7.

Lamberg, I. and Hallström, B. (1986) 'Thermal properties of potatoes and a computer simulation model of a blanching process', *International Journal of Food Science & Technology*, 21(5), pp. 577–585. doi:10.1111/j.1365-2621.1986.tb00396.x.

McGee, H. (2004) *On food and cooking: the science and lore of the kitchen*. Completely rev. and updated. New York: Scribner.

Nukiyama, S. (1934) 'The Maximum and Minimum Values of the Heat Q Transmitted from Metal to Boiling Water under Atmospheric Pressure', *Journal of the Society of Mechanical Engineers*, 37(206), pp. 367–374. doi:10.1299/jsmemagazine.37.206_367.

Singh, R.P. and Heldman, D.R. (2014) 'Heat Transfer in Food Processing', in *Introduction to Food Engineering*. Elsevier, pp. 265–419. doi:10.1016/B978-0-12-398530-9.00004-8.

Sjöö, M. (ed.) (2018) *Starch in food: structure, function and applications*. Second edition. Cambridge, MA, United States: Woodhead Publishing is an imprint of Elsevier (Woodhead Publishing series in food science, technology and nutrition).

Speth, J.D. (2015) 'When Did Humans Learn to Boil?', *Paleo Anthropology*, p. 14.

X. APPENDICES

APPENDIX A

TABLE 1

The zeroth- and first-order Bessel functions of the first kind for calculation of the transcendental equation for transient conduction in an infinite cylinder:

μ	$J_0(\mu)$	$J_1(\mu)$
0	1,0000	0,0000
0,1	0,9975	0,0499
0,2	0,9900	0,0995
0,3	0,9776	0,1483
0,4	0,9604	0,1960
0,5	0,9385	0,2423
0,6	0,9120	0,2867
0,7	0,8812	0,3290
0,8	0,8463	0,3688
0,9	0,8075	0,4059
1	0,7652	0,4400
1,1	0,7196	0,4709
1,2	0,6711	0,4983
1,3	0,6201	0,5220
1,4	0,5669	0,5419
1,5	0,5118	0,5579
1,6	0,4554	0,5699
1,7	0,3900	0,5778
1,8	0,3400	0,5815
1,9	0,2818	0,5812
2	0,2239	0,5767
2,1	0,1666	0,5683
2,2	0,1104	0,5560
2,3	0,0555	0,5399
2,4	0,0025	0,5202
2,6	-0,0968	0,4708
2,8	-0,185	0,4097
3	-0,2601	0,3391
3,2	-0,3202	0,2613

TABLE 2

The first six roots of the transcendental equation for transient conduction in an infinite slab:

$$\mu_n \cdot tan(\mu_n) = Bi$$

Bi	μ_1	μ_2	μ_3	μ_4	μ_5	μ_6
0,001	0,0316	3,1419	6,2833	9,4249	12,5665	15,708
0,002	0,0447	3,1422	6,2835	9,425	12,5665	15,7081
0,004	0,0632	3,1429	6,2838	9,4252	12,5667	15,7082
0,006	0,0774	3,1435	6,2841	9,4254	12,5668	15,7083
0,008	0,0893	3,1441	6,2845	9,4256	12,567	15,7085
0,01	0,0998	3,1448	6,2848	9,4258	12,5672	15,7086
0,02	0,141	3,1479	6,2864	9,4269	12,568	15,7092
0,04	0,1987	3,1543	6,2895	9,429	12,5696	15,7105
0,06	0,2425	3,1606	6,2927	9,4311	12,5711	15,7118
0,08	0,2791	3,1668	6,2959	9,4333	12,5727	15,7131
0,1	0,3111	3,1731	6,2991	9,4354	12,5743	15,7143
0,2	0,4328	3,2039	6,3148	9,4459	12,5823	15,7207
0,3	0,5218	3,2341	6,3305	9,4565	12,5902	15,727
0,4	0,5932	3,2636	6,3461	9,467	12,5981	15,7334
0,5	0,6533	3,2923	6,3616	9,4775	12,606	15,7397
0,6	0,7051	3,3204	6,377	9,4879	12,6139	15,746
0,7	0,7506	3,3477	6,3923	9,4983	12,6218	15,7524
0,8	0,791	3,3744	6,4074	9,5087	12,6296	15,7587
0,9	0,8274	3,4003	6,4224	9,519	12,6375	15,765
1	0,8603	3,4256	6,4373	9,5293	12,6453	15,7713
1,5	0,9882	3,5422	6,5097	9,5801	12,6841	15,8026
2	1,0769	3,6436	6,5783	9,6296	12,7223	15,8336
3	1,1925	3,8088	6,704	9,724	12,7966	15,8945
4	1,2646	3,9352	6,814	9,8119	12,8678	15,9536
5	1,3138	4,0336	6,0096	9,8928	12,9352	16,0107
6	1,3496	4,1116	6,9924	9,9637	12,9988	16,0654
7	1,3766	4,1746	7,064	10,0339	13,0584	16,1177
8	1,3978	4,2264	7,1263	10,0949	13,1141	16,1675
9	1,4149	4,2694	7,1806	10,1502	13,166	16,2147
10	1,4289	4,3058	7,2281	10,2003	13,2142	16,2594
15	1,4729	4,4255	7,3959	10,3898	13,4078	16,4474
20	1,4961	4,4915	7,4954	10,5117	13,542	16,5864
30	1,5202	4,5615	7,6057	10,6543	13,7085	16,7691
40	1,5325	4,5979	7,6647	10,7334	13,8048	16,8794
50	1,54	4,6202	7,7012	10,7832	13,8666	16,9519
60	1,5451	4,6353	7,7259	10,8172	13,9094	17,0026
80	1,5514	4,6543	7,7573	10,8606	13,9644	17,0686
100	1,5552	4.6658	7,7764	10,8871	13,9981	17,1093
∞	1,5708	4,7124	7,854	10,9956	14,1372	17,2788

TABLE 3

The first six roots of the transcendental equation for transient conduction in an infinite cylinder:

$$\mu_n \cdot \frac{J_1(\mu_n)}{J_0(\mu_n)} = Bi$$

Bi	μ_1	μ_2	μ_3	μ_4	μ_5	μ_6
0,01	0,1412	3,8343	7,017	10,1745	13,3244	16,4712
0,02	0,1995	3,8369	7,0184	10,1754	13,3252	16,4718
0,04	0,2814	3,8421	7,0213	10,1774	13,3267	16,4731
0,06	0,3438	3,8473	7,0241	10,1794	13,3282	16,4743
0,08	0,396	3,8525	7,027	10,1813	13,3297	16,4755
0,1	0,4417	3,8577	7,0298	10,1833	13,3312	16,4767
0,15	0,5376	3,8706	7,0369	10,1882	13,3349	16,4797
0,2	0,617	3,8835	7,044	10,1931	13,3387	16,4828
0,3	0,7465	3,9091	7,0582	10,2029	13,3462	16,4888
0,4	0,8516	3,9344	7,0723	10,2127	13,3537	16,4949
0,5	0,9408	3,9594	7,0864	10,2225	13,3611	16,501
0,6	1,0184	3,9841	7,1004	10,2322	13,3686	16,507
0,7	1,0873	4,0085	7,1143	10,2419	13,3761	16,5131
0,8	1,149	4,0325	7,1282	10,2516	13,3835	16,5191
0,9	1,2048	4,0562	7,1421	10,2613	13,391	16,5251
1	1,2558	4,0795	7,1558	10,271	13,3984	16,5312
1,5	1,4569	4,1902	7,2233	10,3188	13,4353	16,5612
2	1,5994	4,291	7,2884	10,3658	13,4719	16,591
3	1,7887	4,4634	7,4103	10,4566	13,5434	16,6499
4	1,9081	4,6018	7,5201	10,5423	13,6125	16,7073
5	1,9898	4,7131	7,6177	10,6223	13,6786	16,763
6	2,049	4,8033	7,7039	10,6964	13,7414	16,8168
7	2,0937	4,8772	7,7797	10,7646	13,8008	16,8684
8	2,1286	4,9384	7,8464	10,8271	13,8566	16,9179
9	2,1566	4,9897	7,9051	10,8842	13,909	16,965
10	2,1795	5,0332	7,9569	10,9363	13,958	17,0099
15	2,2509	5,1773	8,1422	11,1367	14,1576	17,2008
20	2,288	5,2568	8,2534	11,2677	14,2983	17,3442
30	2,3261	5,341	8,3771	11,4221	14,4748	17,5348
40	2,3455	5,3846	8,4432	11,5081	14,5774	17,6508
50	2,3572	5,4112	8,484	11,5621	14,6433	17,7272
60	2,3651	5,4291	8,5116	11,599	14,6889	17,7807
80	2,375	5,4516	8,5466	11,6461	14,7475	17,8502
100	2,3809	5,4652	8,5678	11,6747	14,7834	17,8931
∞	2,4048	5,5201	8,6537	11,7915	14,9309	18,0711

TABLE 4

The first six roots of the transcendental equation for transient conduction in a spherical object:

$$1 - \mu_n cot(\mu_n) = Bi$$

Bi	μ_1	μ_2	μ_3	μ_4	μ_5	μ_6
0,01	0,1730	4,4956	7,7265	10,9050	14,0669	17,2213
0,02	0,2455	4,4979	7,7279	10,9060	14,0676	17,2219
0,04	0,3479	4,5025	7,7305	10,9079	14,0691	17,2231
0,06	0,4214	4,5067	7,7330	10,9096	14,0705	17,2242
0,08	0,4875	4,5113	7,7357	10,9115	14,0719	17,2254
0,1	0,5435	4,5158	7,7383	10,9133	14,0733	17,2266
0,15	0,6625	4,5270	7,7448	10,9179	14,0769	17,2295
0,2	0,7640	4,5385	7,7515	10,9227	14,0806	17,2325
0,3	0,9266	4,5610	7,7646	10,9320	14,0878	17,2384
0,4	1,0541	4,5824	7,7771	10,9409	14,0947	17,2440
0,5	1,1661	4,6043	7,7899	10,9500	14,1018	17,2498
0,6	1,2662	4,6266	7,8030	10,9593	14,1090	17,2557
0,7	1,3614	4,6503	7,8170	10,9692	14,1167	17,2620
0,8	1,4386	4,6715	7,8296	10,9782	14,1236	17,2677
0,9	1,5068	4,6918	7,8417	10,9868	14,1303	17,2732
1	1,5767	4,7144	7,8552	10,9964	14,1378	17,2793
1,5	1,8432	4,8188	7,9189	11,0422	14,1735	17,3085
2	2,0281	4,9128	7,9784	11,0854	14,2073	17,3363
3	2,2887	5,0868	8,0960	11,1726	14,2763	17,3932
4	2,4596	5,2368	8,2075	11,2584	14,3453	17,4506
5	2,5731	5,3571	8,3055	11,3370	14,4097	17,5049
6	2,6570	5,4587	8,3953	11,4120	14,4727	17,5587
7	2,7170	5,5386	8,4710	11,4779	14,5294	17,6077
8	2,7643	5,6062	8,5390	11,5393	14,5834	17,6551
9	2,8071	5,6710	8,6076	11,6036	14,6413	17,7067
10	2,8403	5,7237	8,6660	11,6604	14,6936	17,7542
15	2,9378	5,8904	8,8672	11,8707	14,8992	17,9487
20	2,9863	5,9794	8,9845	12,0046	15,0402	18,0906
30	3,0377	6,0775	9,1213	12,1706	15,2263	18,2889
40	3,0641	6,1292	9,1959	12,2651	15,3374	18,4131
50	3,0795	6,1594	9,2403	12,3225	15,4063	18,4921
60	3,0899	6,1801	9,2709	12,3624	15,4549	18,5486
80	3,1024	6,2049	9,3077	12,4108	15,5144	18,6185
100	3,1102	6,2204	9,3308	12,4414	15,5521	18,6632
∞	3,1102	6,2204	9,3308	12,4414	15,5521	18,6632

APPENDIX B

nr	*Storage Time (days)*	*Thermal conductivity ($Wm^{-1}K^{-1}$)*	*Volumetric specific heat ($Jkg^{-1}K^{-1}$)*	*Thermal diffusivity (m^2s^{-1})*	*Thermal Resistivity (mKW^{-1})*
1	28	0.632	4.02	0.157	158
2	28	0.541	4.10	0.132	184
3	28	0.542	3.77	0.143	184
4	28	0.550	4.22	0.130	181
5	28	0.571	3.97	0.144	175
6	28	0.546	4.39	0.124	183
7	28	0.557	4.39	0.127	179
8	28	0.609	4.49	0.135	164
9	28	0.562	4.31	0.130	177
10	28	0.566	4.90	0.116	176
11	14	0.548	4.10	0.134	182
12	14	0.568	4.35	0.130	175
13	14	0.551	4.22	0.130	181
14	14	0.564	4.32	0.130	177
15	14	0.547	4.20	0.130	182
16	14	0.575	4.08	0.141	174
17	14	0.575	4.18	0.137	173
18	14	0.553	4.17	0.132	180
19	14	0.548	4.69	0.117	182
20	14	0.550	3.99	0.138	181

There is no significant difference in thermal conductivity of 14-day-old potatoes (M = 0,567; SD = 0,030) and 28-day-old potatoes (M = 0,559; SD = 0,011), t-value (12) = 0,958, p-value = 0,360.

There is no significant difference in volumetric specific heat of 14-day-old potatoes (M = 4,255; SD = 0,316) and 28-day-old potatoes (M = 4,235; SD = 0,194), t-value (18) = 0,197, p-value = 0,845.

There is no significant difference in thermal diffusivity of 14-day old potatoes (M = 0,133; SD = 0,011) and 28-day-old potatoes (M = 0,131; SD = 0,006), t-value (18) = 0,449, p-value = 0,658.

There is no significant difference in thermal resistivity of 14-day-old potatoes (M = 176,6; SD = 8,834) and 28-day-old potatoes (M = 179,3; SD = 3,643), t-value (12) = -0,9, p-value = 0,385.

APPENDIX C

Results of interval boiling experiment:

Heating time, t (s)	Average Dfs (mm) (n = 4)	Stand. dev. of Dfs (mm)
60	2,5	0
120	4,1	0
180	5,2	0
240	7,825	0,5230
300	Cannot identify	Cannot identify
360	Cannot identify	Cannot identify

Results of interval simmering experiment:

Heating time, t (s)	Average Dfs (mm) (n = 4)	Stand. dev. of Dfs (mm)
60	2,2	0
120	3,585	0,098
180	4,737	0,075
240	6,645	0,044
300	Cannot identify	Cannot identify
360	Cannot identify	Cannot identify

Results of interval sub-boiling at 85°C experiment:

Heating time, t (s)	Average Dfs (mm) (n = 4)	Stand. dev. of Dfs (mm)
60	2,2	0
120	3,585	0,098
180	4,737	0,075
240	6,645	0,044
300	Cannot identify	Cannot identify
360	Cannot identify	Cannot identify

Results of interval sub-boiling at 90°C experiment:

Heating time, t (s)	Average Dfs (mm) (n = 4)	Stand. dev. of Dfs (mm)
60	2,2	0
120	3,585	0,098
180	4,737	0,075
240	6,645	0,044
300	Cannot identify	Cannot identify
360	Cannot identify	Cannot identify